European Journal of Pharmaceutics and Biopharmaceutics 145 (2019) 98–112

Contents lists available at ScienceDirect

European Journal of Pharmaceutics and Biopharmaceutics

journal homepage: www.elsevier.com/locate/ejpb

Research paper

Rivaroxaban polymeric amorphous solid dispersions: Moisture-induced thermodynamic phase behavior and intermolecular interactions

Afroditi Kapourani, Elisavet Vardaka, Konstantinos Katopodis, Kyriakos Kachrimanis, Panagiotis Barmpalexis*

Department of Pharmaceutical Technology, School of Pharmacy, Aristotle University of Thessaloniki, Thessaloniki 54124, Greece

ARTICLE INFO

Keywords:
Rivaroxaban
Amorphous solid dispersions
Thermodynamic modelling
Flory-Huggins lattice theory
RH-phase diagrams
Molecular dynamics simulations

ABSTRACT

The present study evaluates the physical stability and intermolecular interactions of Rivaroxaban (RXB) amorphous solid dispersions (ASDs) in polymeric carriers via thermodynamic modelling and molecular simulations. Specifically, the Flory-Huggins (FH) lattice solution theory was used to construct thermodynamic phase diagrams of RXB ASDs in four commonly used polymeric carriers (i.e. copovidone, coPVP, povidone, PVP, Soluplus, SOL and hypromellose acetate succinate, HPMCAS), which were stored under 0%, 60% and 75% relative humidity (RH) conditions. In order to verify the phase boundaries predicted by FH modelling (i.e. truly amorphous zone, amorphous-amorphous demixing zones and amorphous-API recrystallization zones), samples of ASDs were examined via polarized light microscopy after storage for up to six months at various RH conditions. Results showed a good agreement between the theoretical and the experimental approaches (i.e. coPVP and PVP resulted in less physically-stable ASDs compared to SOL and HPMCAS) indicating that the proposed FH-based modelling may be a useful tool in predicting long-term physical stability in high humidity conditions. In addition, molecular dynamics (MD) simulations were employed in order to interpret the observed differences in physical stability. Results, which were verified via differential scanning calorimetry (DSC) and Fourier transform infrared spectroscopy (FTIR), suggested the formation of similar intermolecular interactions in all cases, indicating that the interaction with moisture water plays a more crucial role in ASD physical stability compared to the formation of intermolecular interactions between ASD components.

1. Introduction

Until today, the several techniques proposed in order to overcome Active Pharmaceutical Ingredients (APIs) poor aqueous solubility include the preparation of self-emulsifying drug delivery systems, co-crystals, nanocrystals, cyclodextrins etc. [1–8]. Among them, the preparation of amorphous drug solid dispersions (ASD) has gained a wide attention for several years [9–11]. However, despite the enormous effort made (considering the large number of scientific publications and patents published in the last three to four decades) the number of marketed products seems to be rather limited. One explanation, as proposed recently by Edueng et al. [12], is the limited in depth evaluation of such amorphous systems in terms of thermodynamic phase properties, molecular interactions, molecular mobility, re-crystallization kinetics etc. Hence, in order to overcome these limitations, in depth evaluation of such systems in terms of thermodynamic, as well as molecular properties is mandatory.

In general, ASDs may be prepared by various techniques such as solvent- (i.e. spray and freeze drying), temperature- (i.e. melt mixing and hot-melt extrusion, HME) and mechanical- (i.e. milling and cryo-milling) based approaches [12]. Especially in the case of temperature-based approaches, the important advantages (such as being environmental friendly (no organic solvents used during production), having improved process efficiency and good scalability [12–14]) has led to several breakthroughs in the field. During the preparation of such ASDs, the API is usually mixed/extruded with a molten or thermo-softened polymer (or mixture of polymer(s) with other additives, such as plasticizers) for appropriate time. Typical thermoplastic polymers (or co-polymers) used in such processes include polyethylene glycols, povidones (PVP), copovidones (coPVP), hypromelloses and derivatives (such as hypromellose acetate succinate, HPMCAS), polyvinyl caprolactam–polyvinyl acetate–polyethylene glycol graft copolymers (Soluplus®, SOL), polymethacrylate copolymers (i.e. Eudragit® S100 and L100) etc. [15–20]. The selection of an appropriate thermoplastic carrier during the formulation development of a pharmaceutical ASD is a nontrivial procedure that may result in an increased number of several

* Corresponding author.
E-mail address: pbarmp@pharm.auth.gr (P. Barmpalexis).

https://doi.org/10.1016/j.ejpb.2019.10.010
Received 20 August 2019; Received in revised form 19 October 2019; Accepted 22 October 2019
Available online 04 November 2019
0939-6411/

(time and resource consuming) experimental trials.

In this respect, several authors have tried to evaluate the thermodynamic phase behavior of ASD as an attempt to properly select the most appropriate carrier. In most of the cases, a thermodynamic phase diagram of a two component system (API and carrier) is drawn under zero-humidity conditions (conditions prevailing during ASD temperature-based preparations) based on the Flory-Huggins lattice theory, although several other approaches (such as the use Perturbed-Chain Statistical Associating Fluid Theory, PC-SAFT) have been also evaluated [21–24]. Despite the promising results, the majority of these studies fails to evaluate the thermodynamic behavior of ASD during storage (a critical factor for the successful development of an ASD-based product), probably due to the complexity of calculations introduced into the system with the addition of a third component (i.e. moisture water).

Rivaroxaban (RXB, 5-chloro-N-(((5S)-2-oxo-3-[4-(3-oxo-4-morpholinyl) phenyl]-1, 3 oxazolidin-5-yl) methyl)-2-thiophene-carboxamide,) is categorized as a BCS class II API exhibiting poor aqueous solubility and high permeability across the gastrointestinal tract [25]. In order to enhance it's aqueous solubility various attempts, including the preparation of self-micro-emulsifying drug delivery systems and lipid solid dispersion, have been proposed [7,26]. Until today, there has been only one attempt for the preparation of polymeric ASDs containing RXB [27]. In this study, the enhanced biopharmaceutical performance of RXB from polymeric-based ASDs, using polymethacrylate copolymers (Eudragit® S100 and L100) and SOL was shown, with approximately 6-fold increase of both AUC and C_{max} values (for SOL ASDs) compared to pure crystalline API. Hence, since the preparation of polymeric ASDs seems to be a promising approach for RXB's enhanced bioavailability, an evaluation of the thermodynamic phase properties and the interactions at the molecular level is of crucial importance in order to gain an insight into the physical stability of the system.

Therefore, for the first time in the present study the thermodynamic phase properties of RXB using four thermoplastic polymers or copolymers (PVP, coPVP, HPMC-AS and SOL) were evaluated after storage at different RH conditions (i.e. 0% RH prevailing during ASD preparation, and 60% RH and 75% RH commonly occurring during storage stability tests). Specifically, an extension of Flory-Huggins (FH) lattice-based solution theory including a third component (moisture) was evaluated in order to gain an insight and a more realistic perspective into the thermally induced phase transition phenomena occurring during ASD storage. Additionally, in order to evaluate the formation of intermolecular interactions between RXB and the selected polymeric carriers, molecular simulations were employed, and the results were verified via experimental observations.

2. Materials and methods

2.1. Materials

Rivaroxaban (RXB) crystals of form I (the most thermodynamically stable polymorph) were kindly donated by Genepharm S.A. (Athens, Greece), while graft copolymer Soluplus® (SOL), povidone (Kollidon®K25, PVP) and copovidone (Kollidon®VA64, coPVP) were obtained from BASF (Ludwigshafen, Germany), and hypromellose acetate succinate (Aquoat®AS-LF, HPMC-AS) was supplied by Shin-Etsu (Tokyo, Japan). All other reagents were of analytical grade and used as received.

2.2. Preparation of ASD

All RXB polymeric ASD were prepared by the melt-quenching approach. Specifically, accurately weighted amounts of API and the selected polymers were mixed at different weight ratios with a mortar and a pestle and heated up to 250 °C until a homogenous paste-like dispersion was obtained. The resultant dispersion was rapidly cooled in an ice bath and then gently ground and passed through a 300 mm sieve. The prepared samples were placed in hermetically sealed amber glass vials and stored in desiccators at 25 °C in order to prevent moisture absorption prior testing.

2.3. Differential scanning calorimetry (DSC) studies

Thermal analyses were conducted on a heat-flux differential scanning calorimeter (DSC-204 F1 Phoenix, NETZSCH, Germany) calibrated with high purity indium standards. Accurately weighted samples (5.0 ± 0.2 mg) placed in perforated aluminum pans were used, while nitrogen flow was applied in order to provide a constant thermal blanket within the DSC cell. The standard deviations of temperatures determined in this work were not higher than 1.0 °C.

2.4. Miscibility evaluation

In order to evaluate the miscibility of RXB with the selected polymers, the following methods were employed:

2.4.1. FH interaction parameter

The FH interaction parameter χ accounts for the enthalpy of mixing and is an indication of API-polymer miscibility. At low polymer weight fractions the interaction parameter, χ, may be assumed as constant (independent of temperature and volume fraction) and hence it can be calculated from the slope of line derived from the graph of $\Phi^2_{polymer}$ to $\left(\frac{1}{T_{m(mix)}}-\frac{1}{T_{m(pure)}}\right)\left(\frac{-\Delta H_{fus}}{R}\right)-ln\Phi_{RXB}-\left(1-\frac{1}{m}\right)\Phi_{pol}$ [28]. $T_{m(pure)}$ and $T_{m(mix)}$ are the melting temperatures of the pure RXB and of the API in the presence of a matrix carrier, respectively; ΔH_{fus} is the heat of fusion of the pure API, m is the volume ratio of the polymer to API (calculated as molar volumes from the true density values), R is the gas constant, χ is the FH interaction parameter, and Φ_{RXB} and Φ_{pol} are the volume fractions of RXB and matrix carrier, respectively. Negative values of χ indicate miscibility between the API and the tested polymers.

2.4.2. Solubility parameters (δ)

Miscibility of RXB with the tested thermoplastic polymers, was also evaluated with the aid of solubility parameters estimated by the Hoftyzer-Van Krevelen group contribution methods. In general solubility of the API within the polymer matrix is based on the following equation [29]:

$$\ln(\gamma_{RBX})x_{RXB}=ln\Phi_{RXB}+\left(1-\frac{1}{m}\right)\Phi_{polymer}+\chi\Phi^2_{polymer} \quad (1)$$

while, the activity coefficient (γ) in this case is estimated on the basis of the extended Hansen solubility model.

$$\ln(\gamma_{API})=\left\{\frac{V_{API}}{RT}\right\}\{(\delta_d^{API}-\bar{\delta}_d)^2+0.25[(\delta_p^{API}-\bar{\delta}_p)^2+(\delta_h^{API}-\bar{\delta}_h)^2]\}+\ln\left(\frac{V_{API}}{\bar{V}}\right)+1-\frac{V_{API}}{\bar{V}} \quad (2)$$

where $\bar{\delta}$ are molar volume weighted solubility parameters and $\bar{V}$ is the mixture volume derived from the following equations:

$$\bar{\delta}=\sum_{k=1}^{n}\Phi_k\delta_k \quad (3)$$

$$\Phi_k=\frac{x_kV_k}{\bar{V}} \quad (4)$$

$$V_k=\frac{MW_k}{\rho_k} \quad (5)$$

$$\bar{V}=\sum_{k=1}^{n}x_kV_k \quad (6)$$

where, MW the molecular weight, ρ is the density, and the subscript k denotes the different components of the mixture.

2.4.3. Molecular docking simulations

The binding affinity of RXB with the selected thermoplastic polymers, characterizing the mutual solubility of the systems, was estimated via molecular docking simulations.

The initial molecular structures containing 30 monomers of all thermoplastic polymers (PVP, coPVP, HPMC-AS and SOL) were prepared using XenoView v.3.7.9.0 (available online at http://www.vemmer.org/xenoview/xenoview.html). The structure of RXB was taken from PubChem (PubChem CID: 9875401). All materials, treated as non-periodic structures, were optimized (energy minimization) using the pcff_d force field. During geometry optimization tolerance was set at 1.00E−4 kcal/mol, while maximum displacement per iteration was set at 10 Å.

In all molecular docking simulations, the thermoplastic polymers were treated as receptors and the API as ligand taking various orientations against them. AutoDock-Vina software program [30] was used for the preparation of the compound structures (non-polar hydrogen atoms were merged and Kollman united-atom type charges and solvation parameters were added [31]); while the binding affinity values were calculated using an extension of force-field-based scoring functions considering hydrogen bonds, solvation and entropy contributions.

2.4.4. Experimental verification

In order to verify the API-polymer miscibility predictions two experimental approaches were employed:

2.4.4.1. DSC measurements. For the determination of ASD glass transition temperature, and hence the evaluation of miscibility between the API and the selected thermoplastic polymers, DSC studies were conducted using the instrumentation presented in section 2.3. Each sample (physical mixtures of the API and the matrix polymers) was scanned using a cyclic scanning procedure. Specifically, the samples were heated from 20 °C to 250 °C at a heating rate of 10 °C/min and were maintained at that temperature for three (3) min in order to achieve equilibrium and erase any thermal history. Then, the samples were quench-cooled at −30 °C, kept at that temperature for three (3) min and heated again up to 250 °C with 10 °C/min. The glass transition temperature was calculated from the mid-point of the step change in heat flow during the second heating run.

2.4.4.2. Hot-stage polarized light microscopy (HSM). HSM was used also for the evaluation of component's miscibility during melting. Specifically, physical mixtures of RXB with the studied matrix polymers (at a ratio of 40:60 w/w API to polymer) were heated from 25 °C until complete melting (at a rate of 10 °C/min) on a Linkam THMS600 heating stage (Linkam Scientific Instruments Ltd, Surrey, UK), mounted on Olympus BX41 polarized light microscope, and controlled through a Linkam TP94 temperature controller. Evaluation of miscibility was made by optical observation.

2.5. Construction and verification of thermodynamic phase transition diagrams

For the construction of the thermodynamic phase diagrams the melting point depression values of RXB in mixtures of 10:90, 20:80, 30:70, 40:60, 50:50, 60:40, 70:30, 80:20 and 90:10 w/w of API to polymer, were determined via DSC using the instrumentation presented in section 2.3. Specifically, accurately weighted samples (~5.0 mg) were heated from 20 °C to 250 °C at a heating rate of 10 °C/min and the end-set values of RXB endothermic fusion peaks were used for the construction of phase diagrams.

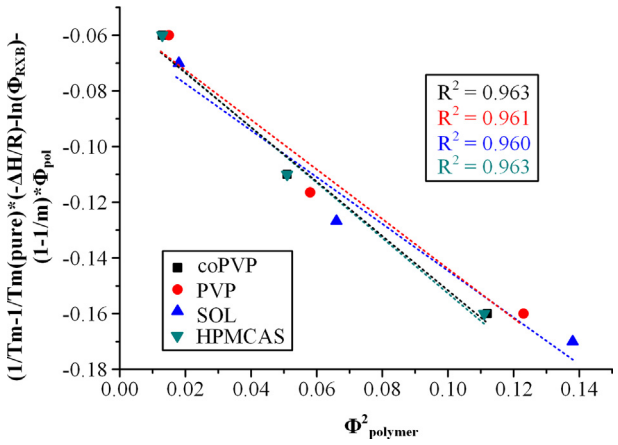

Fig. 1. FH interaction plot used to determine miscibility of component through the interaction parameter, χ, from RXB melting point depression.

2.5.1. Phase diagrams at zero relative humidity conditions

During the preparation of ASD via temperature-based techniques (such as HME) elevated process temperatures (above 100 °C) are commonly employed. In such conditions, zero humidity environment can be assumed, and hence a thermodynamic phase diagram for a typical binary pharmaceutical ASD may consists of [10,32]: (1) a liquid–solid transition curve (liquidus), (2) a spinodal curve (representing the area where two separate phases are observed) and (3) a glass-transition (T_g) curve (showing the boundary between the glassy and rubbery state).

Based on the FH lattice solution theory, the liquidus line at dry (humidity-free) conditions can be estimated by fitting the following equation to the melting point depression data obtained from DSC measurements [10,32]:

$$\left(\frac{1}{T_m(mix)} - \frac{1}{T_m(pure)}\right) = \frac{-R}{\Delta H_{fus}}\left[ln\Phi_{RBX} + \left(1 - \frac{1}{m}\right)\Phi_{pol} + \chi\Phi_{pol}^2\right] \quad (7)$$

where, $T_m(pure)$ and $T_m(mix)$ are the end-set values of the fusion peaks for the pure RXB and of the RXB in the presence of the thermoplastic polymer, respectively; ΔH_{fus} is the heat of fusion of the pure RXB, m is the volume ratio of the polymer to RXB (calculated as molar volumes derived from the true density), R is the gas constant, χ is the FH interaction parameter, and Φ_{RBX} and Φ_{pol} are the volume fractions of RXB and polymer, respectively. In the present study, the FH interaction parameter at zero RH conditions was considered to be dependent only on temperature:

$$\chi = A + \frac{B}{T} \quad (8)$$

where, A is the value of the temperature-independent term (entropic contribution), B is the value of the temperature dependent term (enthalpic contribution). Similarly, the spinodal phase separation curve at dry (humidity-free) conditions is calculated from the second derivative of the FH-based free energy equation [32]:

$$\Delta G = RT\left[\Phi_{RXB}ln\Phi_{RXB} + \left(\frac{1-\Phi_{RXB}}{m}\right)\ln(1-\Phi_{RXB}) + \chi\Phi_{RXB}(1-\Phi_{RXB})\right] \quad (9)$$

Finally, in order to obtain the glassy-rubbery phase boundary line the Gordon–Taylor equation was used according to the following equations [33]:

$$T_g = \frac{\sum K_i w_i T_{g,i}}{\sum K_i w_i} \quad (10)$$

$$K = \frac{\rho_{API} T_{g,API}}{\rho_i T_{g,i}} \quad (11)$$

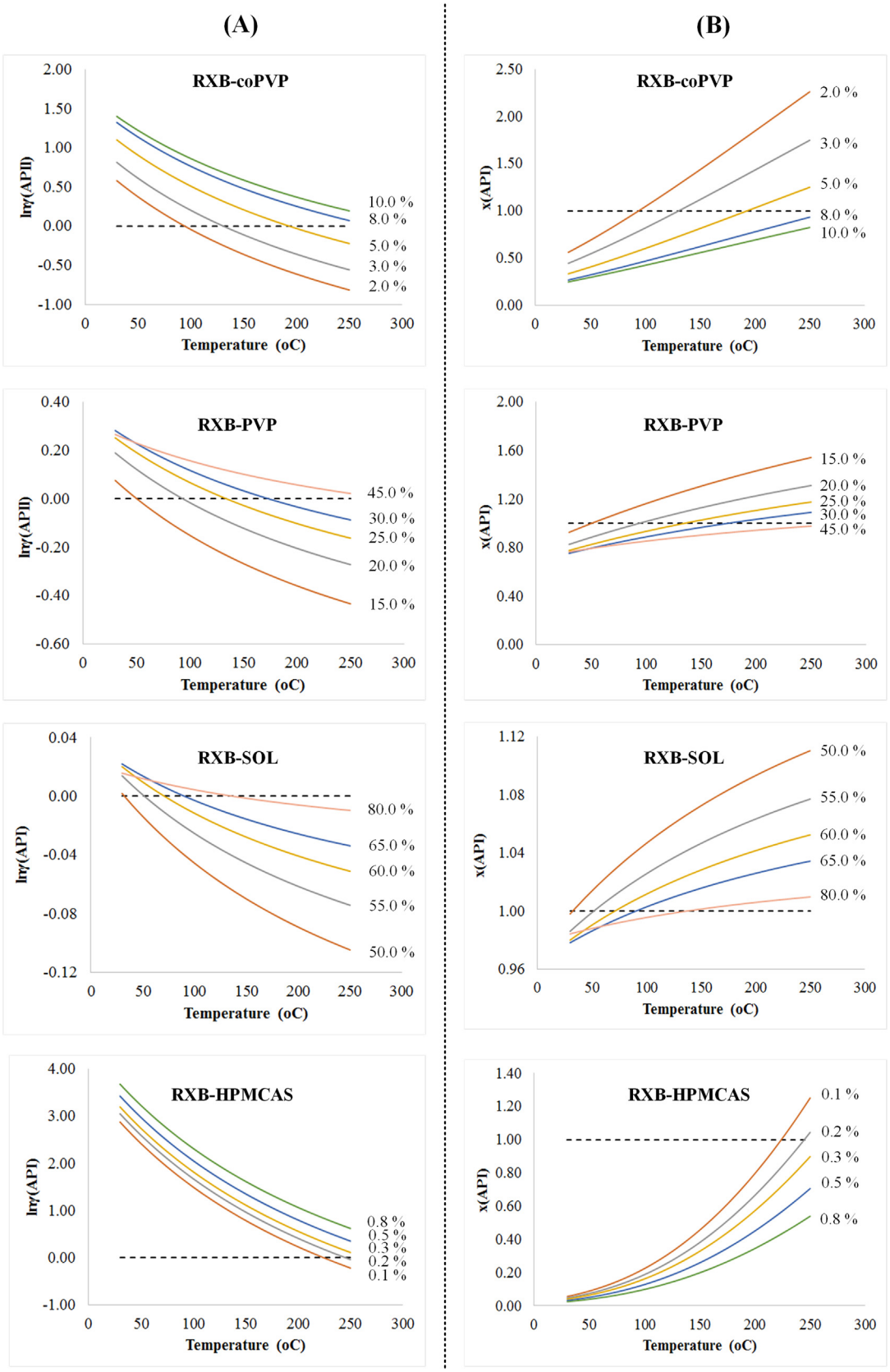

Fig. 2. Changes in activity coefficient (A) and mole fraction (B) (percentages in the legend correspond to the weight fraction of RXB in the mixtures). Horizontal dashed lines represent the case of ideal mixing ($\ln\gamma = 0$).

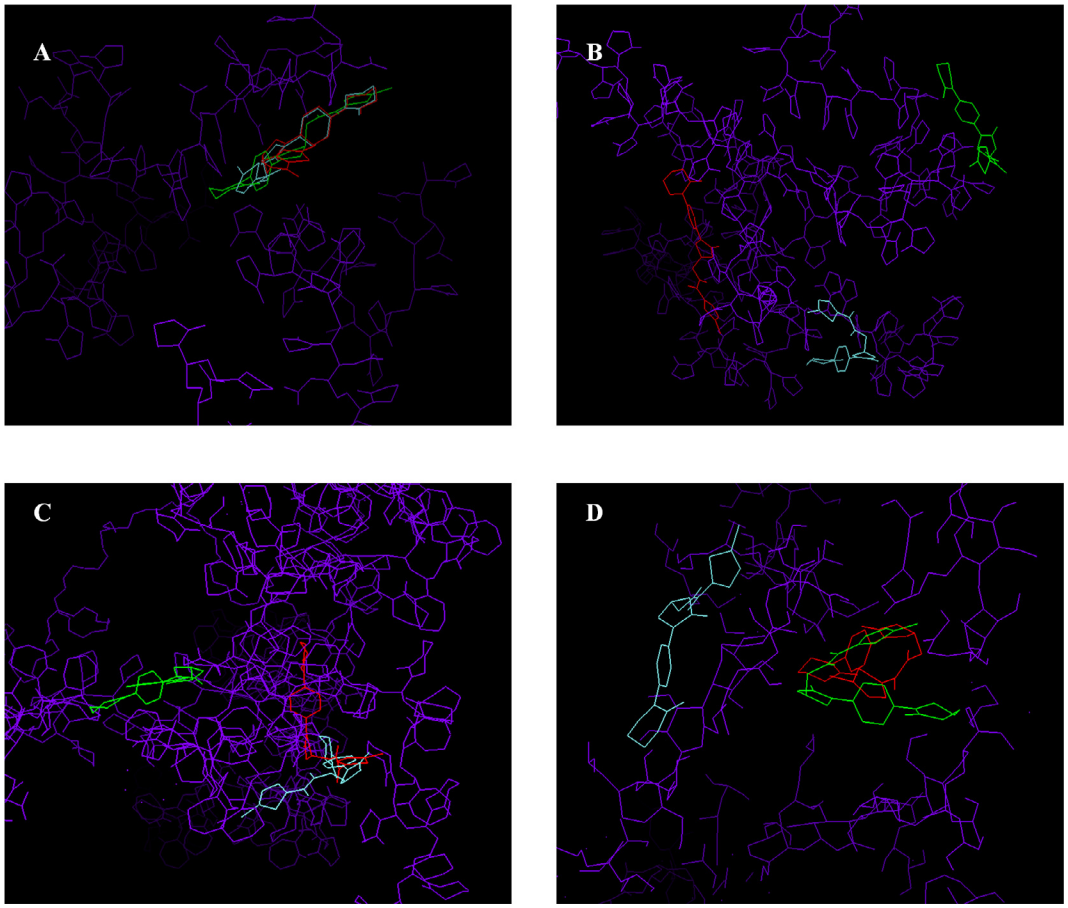

Fig. 3. Three most stable RXB-polymer poses predicted by molecular docking simulations: RXB-coPVP (A), RXB-PVP (B), RXB-SOL(C) and RXB-HPMCAS (D). All polymers are depicted with purple. (For interpretation of the references to color in this figure legend, the reader is referred to the web version of this article.)

where T_g is the glass transition of the blend, w_i are the overall weight fractions of the neat components forming the blend, T_{gi} are the glass transition temperatures of components, K is a constant representing a semi-quantitative measure of the interaction strength between the functional groups, and ρ_i are the densities of each component (determined experimentally with a helium pycnometer, Ultrapycnometer 1000, Quantachrome Instruments, USA).

2.5.2. Phase diagrams at elevated RH conditions

In order to predict RXB physical state during storage stability testing, the thermodynamic phase behavior of the API should be evaluated in regards to RH. Hence, a system with three components (i.e. the API, the polymer and moisture water) and three phases (vapor, *V*, solid, *S*, and liquid, *L*) should be considered. The basic assumptions made in this context are [21,34,35]: (1) vapor phase is assumed to consist of pure water (vapor pressure of API and polymer(s) are negligible compared to vapor pressure of water), (2) solid phase is assumed to consist of pure (re-crystallized) API, (3) liquid phase is a mixture of water, polymer (all polymers in the present study are amorphous) and dissolved (amorphous) API. Hence, based on the above assumptions, RXB solubility in a mixture of a thermoplastic polymer and (absorbed) water may be calculated by the following equation:

$$x_{RBX}^{L} = \frac{1}{\gamma_{RBX}^{L}} \exp\left[-\frac{\Delta H_{RXB}^{SL}}{RT}\left(1-\frac{T}{T_{RXB}^{SL}}\right)-\frac{\Delta Cp_{RXB}^{SL}}{R}\left(\ln\left(\frac{T_{RXB}^{SL}}{T}\right)-\frac{T_{RXB}^{SL}}{T}+1\right)\right] \quad (12)$$

where x_{RXB}^{L} is the API solubility in the mole fraction, and R is the universal gas constant ($8.3145\ \mathrm{J\,K^{-1}mol^{-1}}$), T_{RXB}^{SL} is the melting temperature of API, ΔH_{RXB}^{SL} is the heat of fusion of API, ΔCp_{RXB}^{SL} is the difference in the solid and liquid heat capacities of the API determined by DSC, and γ_{RBX}^{L} is the activity coefficient of the API in the liquid phase, which is a function of temperature and composition given from the following equations based on FH- lattice solution theory [36]:

$$\begin{aligned} ln\gamma_{RBX}^{L} &= 1 + ln\frac{r_{RXB}}{\bar{r}} - \frac{r_{RXB}}{\bar{r}} + \chi_{RXB,pol}\Phi_{pol}^{2} + r_{RXB}\chi_{RXB,water} \\ &\quad \Phi_{water}^{2} + (\chi_{RBX,pol} - r_{RXB}\chi_{pol,water} + r_{RXB}\chi_{API,water})\Phi_{water}\Phi_{pol} \end{aligned} \quad (13)$$

where, $\chi_{RXB,pol}$, $\chi_{RXB,water}$ and $\chi_{pol,water}$ are the FH interaction parameters of API-polymer, API-water and polymer-water, calculated by the fitting of FH-equation to the DSC melting depression data ($\chi_{RXB,pol}$ assumed independent of T and Φ_i), the RXB-water solubility data used from Sun et al. [37] ($\chi_{RXB,water}$, assumed dependent on T) and the polymer-water isotherms derived from literature [38–40] ($\chi_{pol,water}$ assumed independent of T and Φ_i), respectively. Also, $\bar{r}$, r_{RXB} and r_{pol} in Eq. (13) are segment numbers calculated from densities, ρ, and molar masses (*M*) based on the following equations [36]:

$$\bar{r} = x_{water} + x_{RXB}r_{RXB} + x_{pol}r_{pol} \quad (14)$$

$$r_{RXB} = \frac{M_{RXB}\rho_{water}}{M_{water}\rho_{RXB}} \quad (15)$$

$$r_{pol} = \frac{M_{pol}\rho_{water}}{M_{water}\rho_{pol}} \quad (16)$$

In order to introduce moisture water into the system, the equation of relative humidity (RH) for partial pressure is used:

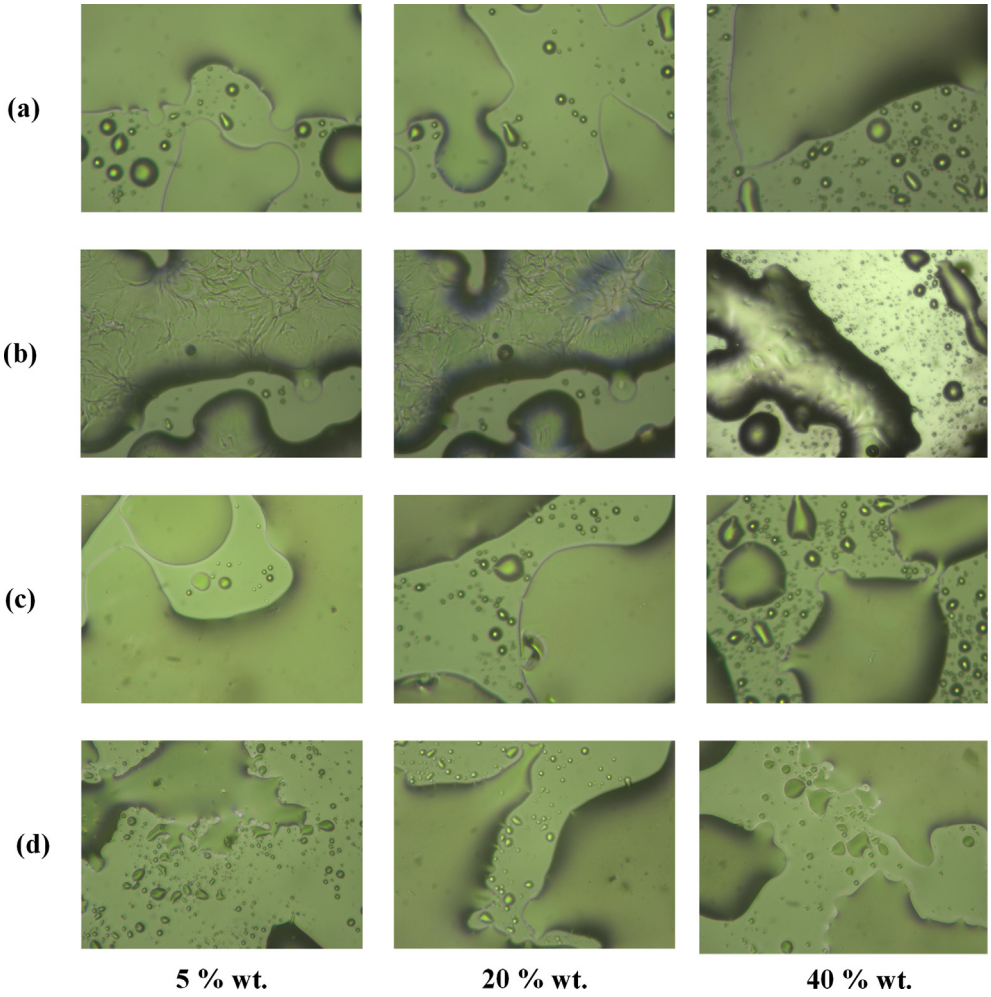

Fig. 4. HSM micrographs obtained under polarized light for RXB-coPVP (a), RXB-PVP (b), RXB-SOL (c), and RXB-HPMCAS (d) mixtures at 5%, 20% and 40% wt. of API.

$$RH = \frac{p^V_{water}}{p^L_{water}} \times 100\% = \gamma^L_{water} \times x^L_{water} \quad (17)$$

where, p^V_{water} is the water partial pressure in the vapor phase, p^L_{water} vapor pressure of pure water at the same temperature, x^L_{water} and γ^L_{water} are the mole fraction and the activity coefficient of water in the liquid phase, respectively. Based on FH-lattice theory the activity coefficient of water is calculated from the following equation:

$$ln\gamma^L_{water} = 1 + ln\frac{1}{\bar{r}} - \frac{1}{\bar{r}} + \chi_{pol,water}\Phi^2_{pol} + \chi_{RXB,water}\Phi^2_{RXB} + (\chi_{pol,water} - \frac{\chi_{RXB,pol}}{r_{RXB}} + \chi_{RXB,water})\Phi_{RXB}\Phi_{pol} \quad (18)$$

Hence, from Eqs. (6) and (11) the amount of absorbed water x^L_{water} as well as the solubility of the API in the polymer/water mixture (x^L_{RXB}) are calculated simultaneously for a given temperature and RH.

Finally, glass-transition (T_g) curve dependence on RH is calculated based on the Gordon-Taylor approach (Eqs. (10) and (11)) taking into account the calculated water content of ASDs from Eq. (17).

2.5.3. Experimental verification of the phase diagrams

In order to verify the suggested phase boundary curves obtained by FH theory, samples of ASD containing either 5.0% or 40.0% of RXB prepared on microscope slides were placed (25 °C) in desiccators at 0% RH (P_2O_5), 60% RH (saturated aqueous NaBr solution) and 75% RH (saturated aqueous NaCl solution), respectively. For comparison, pure RXB (after melting on a microscope slide) was also stored and evaluated at the same conditions. All samples were verified for being amorphous before setting into storage via polarized light microscopy (Olympus BX41). Observations were videotaped with a Jenoptik ProgRes C10Plus color video camera (JENOPTIK Optical Systems GmbH, Jena, Germany) directly attached to the microscope. Evaluation of crystal growth of the stored samples were made up to six (6) months of storage.

2.6. Molecular interactions

The molecular interactions occurring between the API and the thermoplastic polymers during the melt-mixing procedure were evaluated initially on a theoretical base with molecular dynamics (MD) simulations, while DSC and Attenuated Total Reflectance (ATR) FTIR spectroscopy were used in order to experimentally verify the MD simulation findings.

2.6.1. Molecular dynamics (MD) simulations

Xenoview amorphous builder was used to generate the amorphous molecular structure of all tested polymers by packing the structures in a periodic box with a desired density [41] and then RXB molecules were added (at 10 wt.%). The total energy of 10 independently generated simulation boxes was minimized using the pcff_d force field and the structure with the lowest energy was further relaxed by molecular dynamics for 2 ns using the NPT ensemble at atmospheric pressure

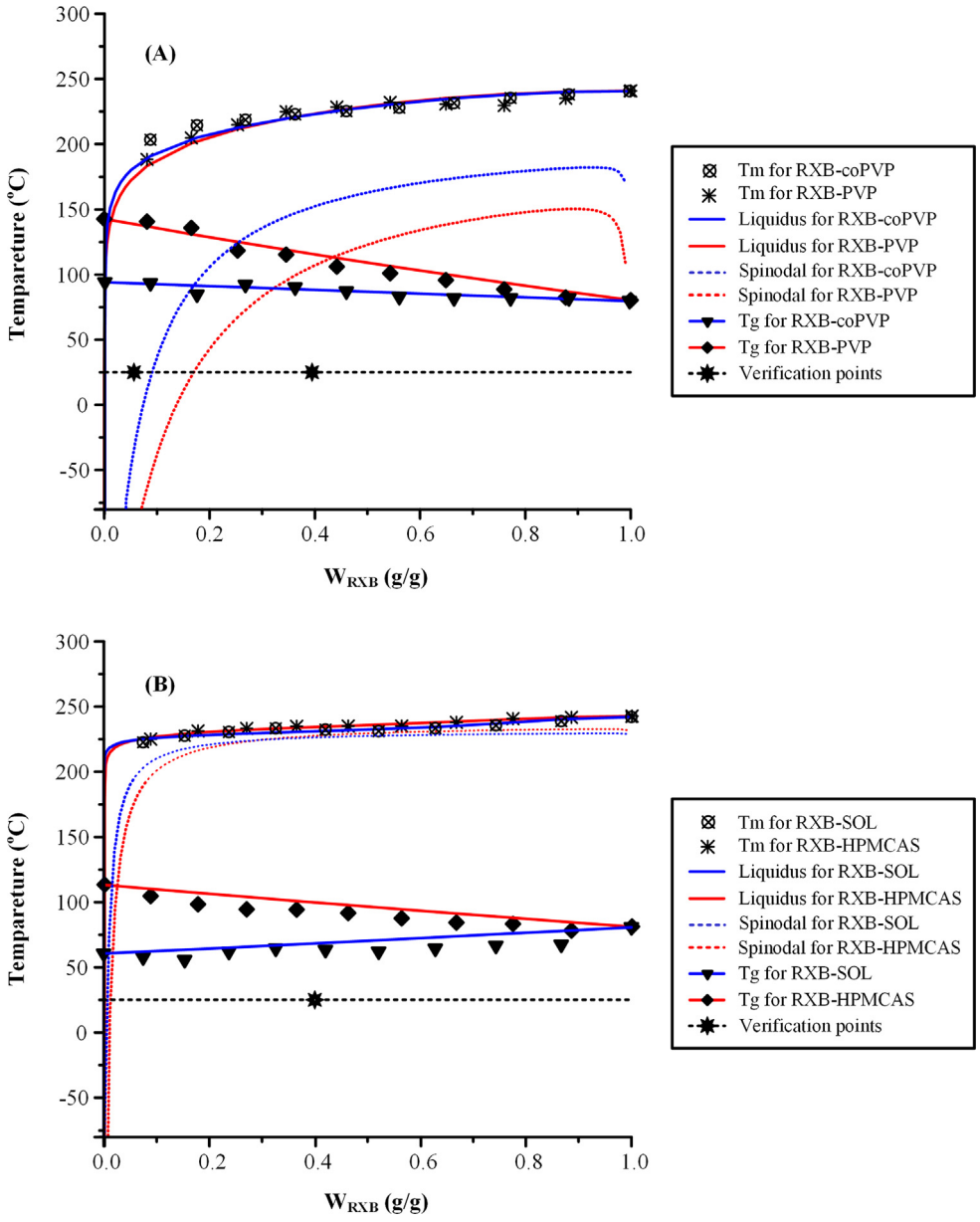

Fig. 5. Binary phase diagrams of RXB-coPVP and RXB-PVP (A) and RXB-SOL and RXB-HPMCAS (B). Black dashed lines represent the storage temperature (25 °C) while the star points on this line show the stability verification check points.

(101.325 kPa) and 250 °C (523.15 K) to obtain a well-relaxed structure with the correct density using a cut-off radius of 7 Å, spline distance of 1 Å, Berendsen thermostat, variable volume and shape option and 1 fs time step. In order to ensure the validity of the simulation the criteria suggested by van Gunsteren and Mark were taken into account for model development, force field selection, sampling scheme setup, and software selection/usage [42].

2.6.2. DSC measurements

In order to evaluate for molecular interactions between RXB and the selected thermoplastic polymers, the experimentally determined Tg values obtained by DSC in section 2.4.3.1, were compared to the Gordon-Taylor theoretically determined Tg values (Eq. (10) and (11)).

2.6.3. Attenuated total reflectance FTIR spectroscopy (ATR-FTIR)

ASD molecular interactions were experimentally evaluated with the aid of ATR-FTIR spectroscopy. Specifically, the FTIR spectra of pure components, physical mixtures and the prepared ASDs in the region of 600–4000 cm^{-1} were obtained using a Shimadzu IR-Prestige-21 FT-IR spectrometer coupled with a horizontal Golden Gate MKII single-reflection ATR system (Specac, Kent, UK) equipped with ZnSe lenses after appropriate background subtraction. Sixty-four (64) scans over the selected wave number range at a resolution of 4 cm^{-1} were averaged for each sample.

3. Results and discussion

3.1. Miscibility evaluation

Miscibility of API with the thermoplastic polymers during the preparation of any ASD system is of crucial importance, especially when screening several suitable polymeric carriers. Hence, the identification of a suitable theoretical and/or experimental approach for doing so is essential.

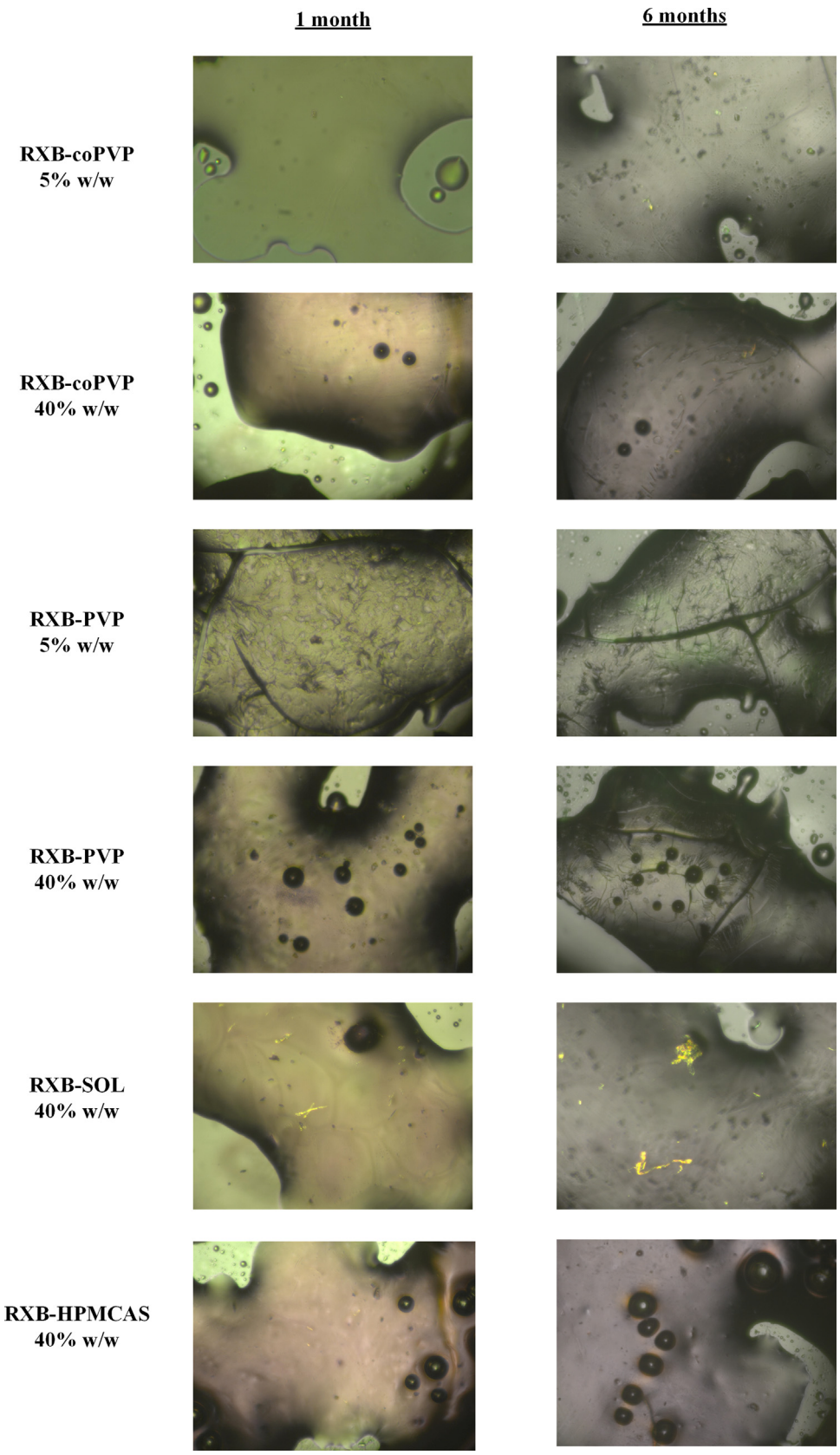

Fig. 6. ASD microscopy images under polarized light after one and six months of storage at zero RH conditions.

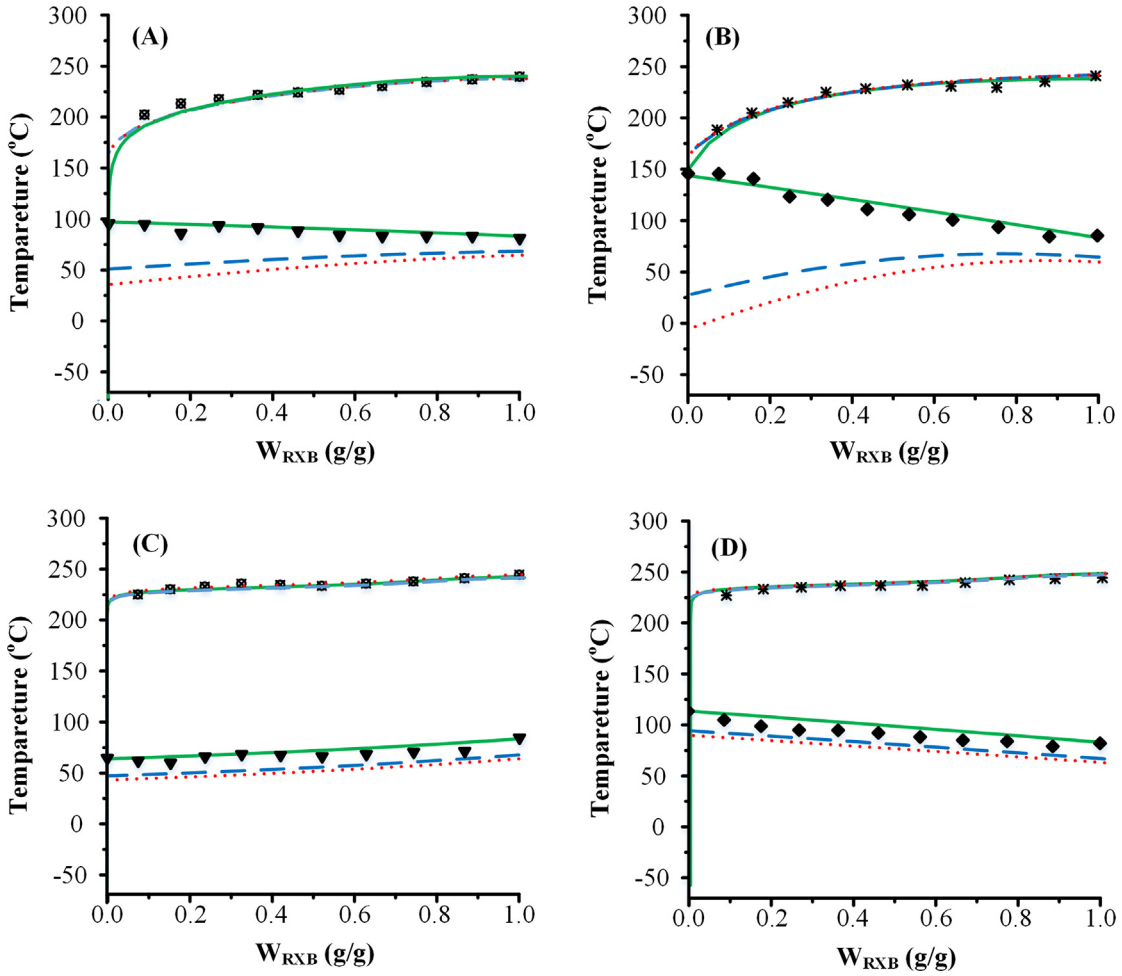

Fig. 7. Effect of RH on the phase behavior of RXB-coPVP (A), RXB-PVP (B), RXB-SOL (C) and RXB-HPMCAS (D) ASDs. Full (green), dashed (blue) and dotted (red) lines reflect 0%, 60% and 75% RH, respectively. (For interpretation of the references to color in this figure legend, the reader is referred to the web version of this article.)

3.1.1. FH interaction parameter

Fig. 1 shows the plots of Φ_{pol}^2 vs. $(1/T_m - 1/T_{m(RXB)})*(-\Delta H/R) - \ln(\Phi_{RXB}) - (1 - 1/m) * \Phi_{pol}$ for all studied systems in low polymer concentrations where the FH-interaction parameter may be considered as independent of both temperature and concentration. The χ values calculated from the slope of the obtained regression lines were -0.932 ($R^2 = 0.963$), -0.848 ($R^2 = 0.961$), -0.897 ($R^2 = 0.960$) and -0.945 ($R^2 = 0.963$) for RXB-coPVP, RXB-PVP, RXB-SOL and RXB-HPMSAC, respectively, indicating that the API is thermodynamically miscible with all studied components (negative χ values in all cases).

3.1.2. Activity coefficient (γ) calculations

Temperature-related miscibility was evaluated theoretically on the basis of activity coefficients using Hansen's solubility parameters. Generally, in ideal mixing γ is considered equal to 1 (consequently, $\ln\gamma = 0$), while when $\ln\gamma < 0$ a solid miscible solution may be feasible [43].

Fig. 2(A) shows the activity coefficient of RXB vs. temperature plots for different weight fractions of API to polymer (coPVP, PVP, SOL and HPMCAS) along with the ideal mixing line ($\ln\gamma = 0$). Figure analysis indicates that in all cases $\ln\gamma$ curves cross the ideal mixing line ($\ln\gamma = 0$) as temperature increases, indicating a strong correlation between miscibility and temperature. Additionally, decreasing amounts of RXB result in lower $\ln\gamma$ values, indicating a strong correlation between RXB's concentration and activity coefficient (better miscibility is obtained at lower RXB concentrations). Furthermore, from the same figure it is concluded that in the case of RXB-SOL miscibility between the two components can be achieved even in high API concentrations, with approximately 80.0% w/w of the API appearing to be miscible at 150 °C, a temperature that is generally regarded acceptable for temperature-based ASD preparation processes (such as HME). At the same temperature, RXB shows moderate solubility in PVP (~25.0% w/w), while only 3.0% of API is miscible in co-PVP, and extremely low miscibility (< 0.1% w/w) is predicted in the case of HPMCAS.

Fig. 2(B) shows the plots of the mole fraction of dissolved RXB, $x_{(API)}$, against temperature, based on Eq. (1). Results show a strong temperature and composition dependence for $x_{(API)}$ in the case of coPVP, SOL and HMPCAS mixtures, with RBX mole fraction values increasing as temperature increases and decreasing as the content of API increases; while, $x_{(API)}$ in RXB-PVP mixtures did not show the same strong temperature or concentration dependence as in the rest of the polymers.

3.1.3. Molecular docking simulations

During molecular docking simulations the estimated binding affinity scores varied from -6.6 to -6.3, -6.4 to -5.5, -6.5 to -6.3 and -5.0 to -4.5 kcal/mol for coPVP, PVP, SOL and HPMCAS mixtures, respectively. In general, since negative binding affinity values indicate strong interactions (and miscibility) among components, it can be concluded that molecular docking simulations predict that the API is miscible with all selected polymeric matrices. However, based on the three (3) most stable RXB-polymer poses derived from the molecular

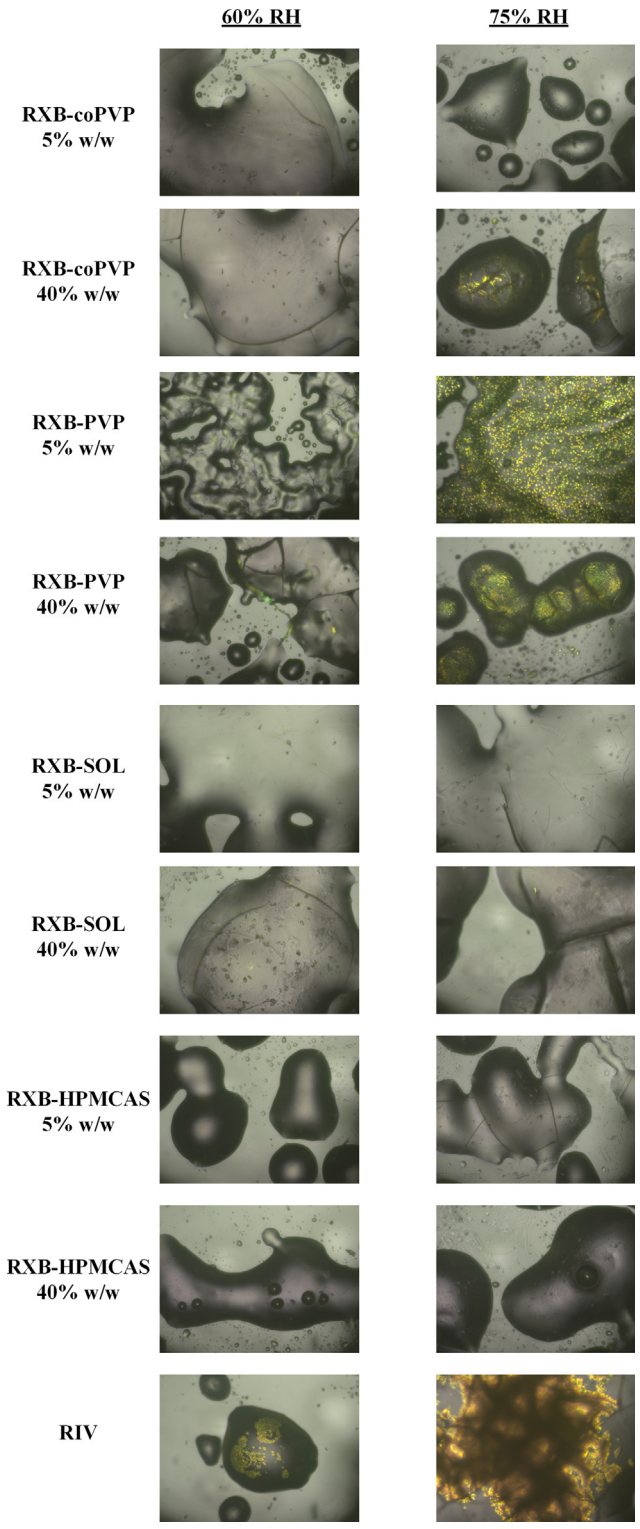

Fig.8. ASD microscopy images under polarized light after six months of storage at 60% and 75% RH.

docking simulations (Fig. 3), in contrast to coPVP, SOL and HPMCAS mixtures, the most stable API conformations in the case of PVP are located on the edge of the polymer (not in the center), indicating that probably API's mixing with PVP is not highly favorable compared to the rest of the polymers.

3.1.4. DSC measurements

In order to verify the above theoretical miscibility results, DSC experiments was conducted. Figure S1 (supplementary) shows the DSC thermograms of the 2nd heating scans for all RXB-polymer mixtures, where a single Tg was recorded in all cases, indicating that the two components (RXB and polymers) are miscible. This is in agreement with the FH and the molecular docking results, where components' miscibility was suggested in all cases.

3.1.5. HSM measurements

Based on a number of recently published reports, DSC's ability (i.e. identification of a single Tg value) to evaluate miscibility of components in ASD systems possesses several drawbacks [44,45]. As an alternative, several other techniques have been proposed, such as XRD and solid-state NMR. Among them, the most promising and easiest to implement is HSM. Fig. 4 shows the HMS micrographs of all RXB-polymer systems at several API to thermoplastic polymer mixtures (i.e. 5%, 20% and 40% w/w of RXB to polymer). In all cases, no API crystals were observed indicating that RXB is dispersed in amorphous state within the selected thermoplastic polymers during the preparation of ASDs. Additionally, based on the obtained results, miscibility between RXB and tested polymers was observed only in three (3) out of the four (4) cases. Specifically, the API was miscible with coPVP, SOL and HPMCAS, while immiscible blends were observed in the case of PVP, where two distinct liquid zones (an API and a polymer zone) were observed. This results indicate that both theoretical predictions and experimental verification via DSC were not suitable to adequately predict API's miscibility (or immiscibility) within the melted thermoplastic polymers, while HMS is a more suitable technique. Nevertheless, it is important to note that molecular docking simulations for RXB and PVP showed that the API's most stable poses are located near polymer's edges, indicating that, if used with caution, molecular docking simulatons may result in scientifically sound conclusions.

3.2. RXB-polymer phase diagrams

3.2.1. Moisture-free phase diagrams

In order to construct the RXB-polymer binary phase diagrams at zero RH conditions the DSC melting point depression data from Figure S2 (supplementary material) were fitted to Eqs. (7) and (8). Based on the fitting results, entropic constant A was calculated at −9.36, −5.14, −114.30 and −68.62, the enthalpic constant B at 4526, 2444, 57,408 and 34772 K for RXB-coPVP, RXB-PVP, RXB-SOL and RXB-HPMCAS, respectively, while good correlation coefficient values were obtained in all cases ($R^2 > 0.95$). Results clearly showed higher entropic and enthalpic contribution in the mixing process of RXB with SOL and HPMCAS, while in the case of RXB-PVP the lowest absolute A and B values were recorded, which is in agreement with the immiscibility of the two components shown previously by HSM.

In a further step, in order to evaluate the combined effect of temperature and composition in the phase transition profile of the selected systems, binary phase diagrams (T vs. API weight fraction) were constructed (Fig. 5) using the parameters listed in Table S1 (supplementary material). In general, temperature-composition phase diagrams are used in order to predict drug's maximum solubility and amorphous miscibility. The liquidus curve (drug solid–liquid phase boundary) shows the fraction of the crystalline API dissolving into the matrix polymer; while the spinodal curve separates two distinct zones [43]: (1) the so-called "unstable" zone on the right-hand-side of spinodal curve, where, from a thermodynamic perspective, phase separation between the API and the polymer is likely to occur and (2) the "metastable" zone on the left-hand-side of spinodal curve until liquidus, where API's nucleation and crystal-growth (the so called re-crystallization process) may be prevented by the implementation of a "supercooling" process and the presence of the thermoplastic polymer which may possess a significant kinetic barrier to API's recrystallization (at least over pharmaceutically relevant time scales, i.e. one (1) to three (3) years). In this metastable zone the prepared binary mixture may remain crystal-free if

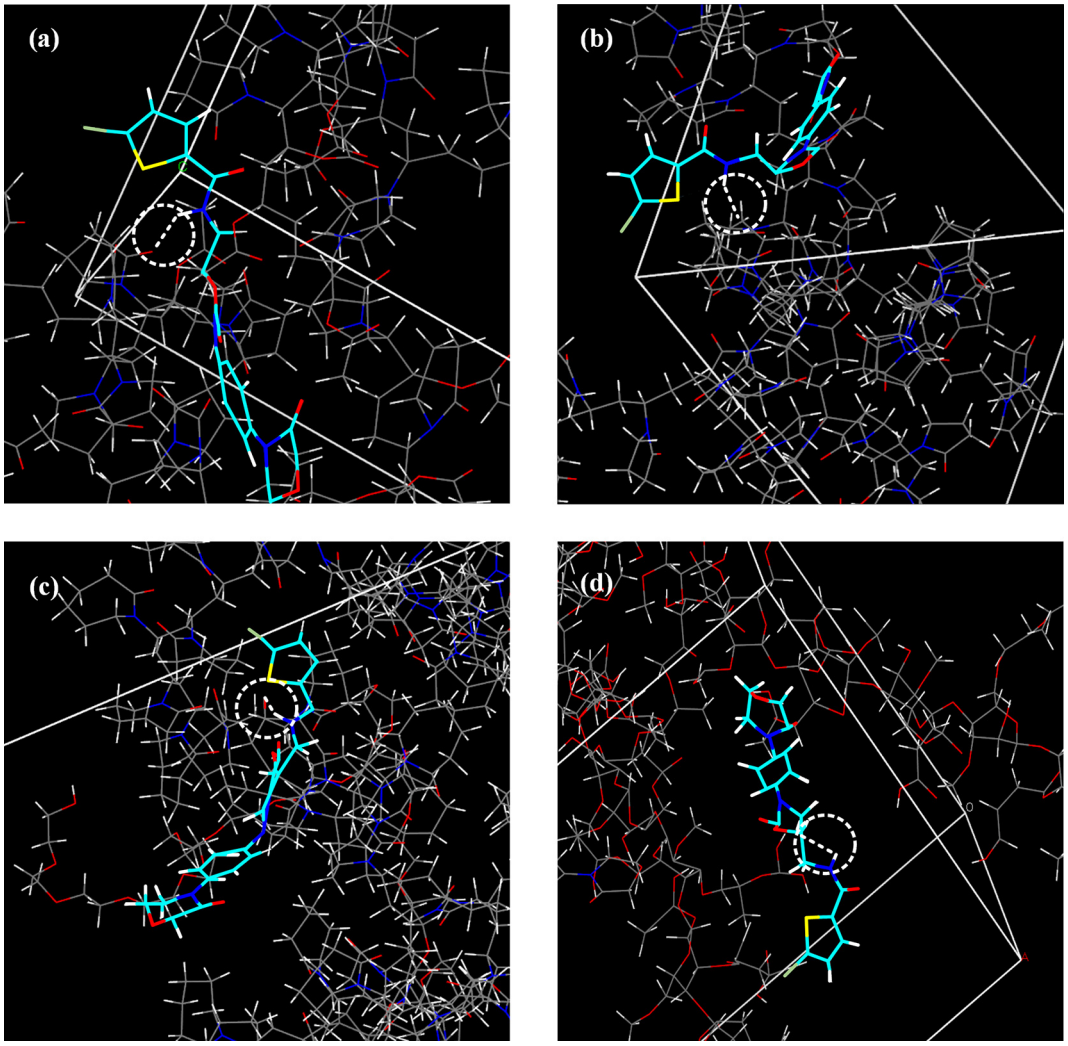

Fig. 9. Representative observed molecular interactions (H-bonds in white dashed circles) for the RXB-coPVP (a), RXB-PVP (b), RXB-SOL (c) and RXB-HPMCAS (d) during MD simulations.

engineered appropriately. Results from figure showed that according to FH lattice theory, in the case of coPVP and PVP (Fig. 5A) a much wider metastable zone is formed compared to SOL and HPMCAS (Fig. 5B). Specifically, at 25 °C (a temperature where most of the orally administrated pharmaceutical products are stored) the metastable zone in RXB-PVP mixtures is extended up to approximately 17% w/w (API to PVP), while for RXB-coPVP mixtures this is restricted to ~8% w/w. On the contrary, both RXB-SOL and RXB-HPMCAS showed a highly restricted metastable zones, located below 0.05% w/w of API to polymer.

In a further step, in order to verify the phase transition boundaries predicted by the FH phase diagrams at zero-humidity, samples of ASD containing either 5.0% w/w (metastable zone) or 40.0% w/w (unstable zone) of RXB were placed in desiccators at 25 °C and 0% RH. In the case of RXB-SOL and RXB-HPMCAS, since the metastable zone is actually extremely restricted, only one sample at 40.0% w/w (unstable zone) was evaluated. Fig. 6 shows the polarized light microscopy images after storage for up to six (6) months. Results showed that in the case of samples located at the thermodynamic "unstable" zone (i.e. 40% w/w of RXB) demixing zones were formed within the first month of storage, indicating that a phase separation process between the API and the polymers occurred rather quickly. These demixing was induced after six (6) months of storage, while in the case of RXB-SOL ASDs, a clear API recrystallization was also observed. On the contrary, in the case of RXB-coPVP samples located at the thermodynamic "metastable" zone (i.e. 5% w/w of RXB), no signs of compounds demixing were observed within the first month of storage, while a rather restricted phase separation was observed after six months. Finally, in the case of RXB-PVP samples with low API content (5% w/w of RXB) located in the "metastable" zone, since the two compounds (API and polymer) were immiscible, some small API recrystallization was observed after six months of storage, which however, was much lesser compared to the samples located in the "unstable" zone.

3.2.2. *Phase diagrams in the presence of moisture*

Fig. 7 shows the RXB-polymer binary phase diagrams at different RH values. In regards to API solubility, results show a small shift on the left of the liquidus line (reduction of solubility) with increasing RH values. This can be attributed to the low API solubility (< 0.01 mg/mL at 25 °C [37]) which leads to an overall reduction of RXB's solubility in the mixture of polymer - water formed in the presence moisture. The reduction of RXB solubility is slightly lower in the case of HPMCAS compared to the rest polymers, probably due to HPMCAS's lower hydrophilicity.

In regards to Tg-curve (which is crucial for the kinetic stability of the amorphous RXB dispersion) increasing RH values led to a downward shift of the curve, especially in the case of RXB-coPVP and RXB-PVP. This shift may be attributed to the extremely low Tg value of water which alters the overall Tg value of the ternary system (API-polymer-moisture water). In all cases, increasing RH values (from 0% to 60% to 75% RH) led to a more significant drop for the kinetic stability curve,

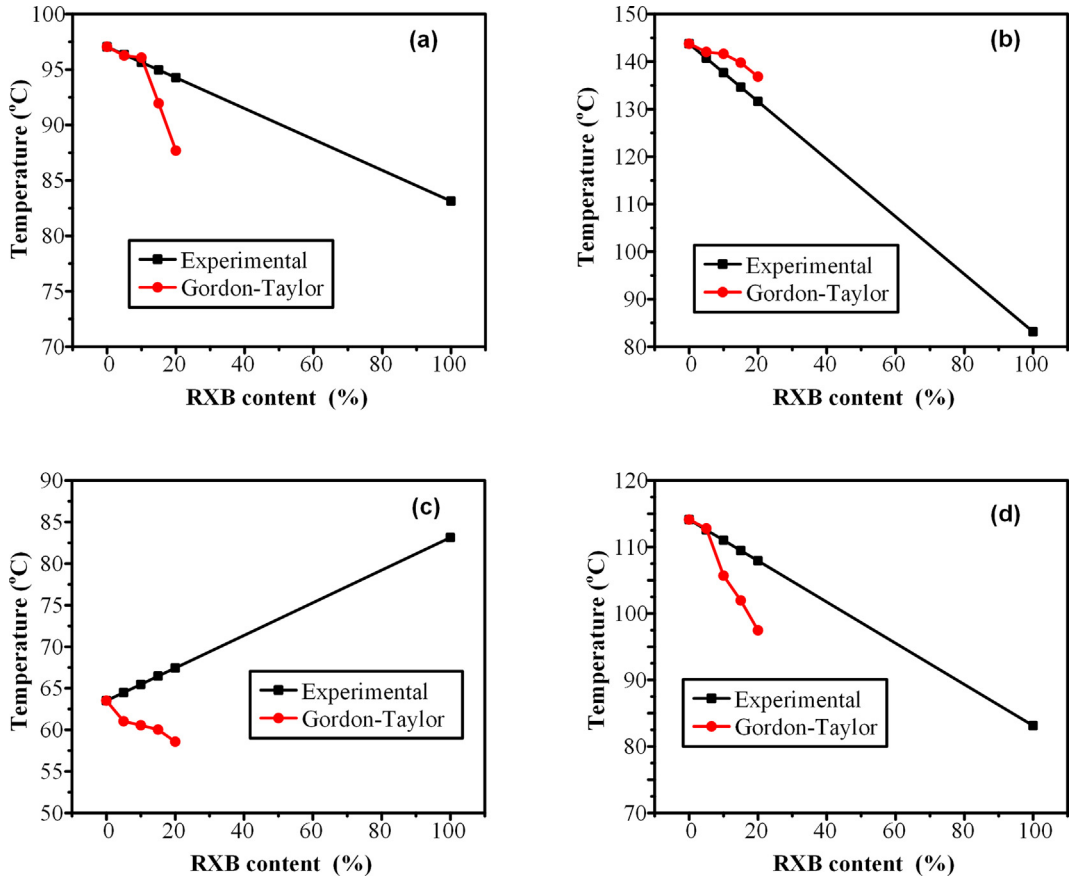

Fig. 10. Prediction of the Tg-composition dependence in all ASD using the Gordon-Taylor equation in comparison with the experimentally determined results for RXB-coPVP (a), RXB-PVP (b), RXB-SOL (c) and RXB-HPMCAS (d).

while increasing amounts of RXB led to higher kinetic stability (less drop of the Tg-curve). The latter, can be attributed to the high hydrophobic nature of RXB, which prevents water moisture penetration into the ASD system leading to higher kinetic stability. As the API's content decreases, and the binary ASD system is getting richer in polymer content, a higher drop of the kinetic stability curve is observed. At this polymer rich regions (above 50% wt. of polymer) the impact of RH on the Tg of the ASDs is more pronounced in the cases of RXB-coPVP and RXB-PVP. This is attributed to the remarkably different hydrophilicity properties of the polymeric carriers with HPMCAS and SOL absorbing only ~ 5.0 wt% and ~ 10.0 wt% of water at 75% RH, respectively, compared to coPVP and PVP which absorb ~ 20.0 wt%, ~50.0 wt% of water at the same conditions. Hence, it seems that the hydrophilicity of the matrix carrier is of crucial importance for achieving kinetic stability during storage under increased RH conditions.

As in the case of zero RH, in order to verify the phase transition boundaries predicted by the FH phase diagrams, samples of ASD containing either 5.0% w/w or 40.0% w/w of RXB were placed in desiccators at 25 °C. Fig. 8 shows the polarized light microscopy images after storage for six (6) months in 60% RH and 75% RH. Results for 60% RH showed that all ASDs were able to stabilize (within a certain level) the API compared to pure RXB (where the API was clearly recrystalized). Additionally, comparison among the ASDs images showed the formation of RXB crystals only in the case of RXB-PVP ASDs containing high amounts of API (40 %wt.), while the formation of demixing zones (amorphous – amorphous) was observed in all high API content ASDs. Furthermore, in the case of 75% RH, HSM images showed that SOL and HPMCAS were able to prevent RXB's recrystallization in contrary to coPVP and PVP where API crystals were formed during storage. This was in accordance with predicted FH phase diagrams where a significant shift of the kinetic stability curve (i.e. Tg-curve) was predicted in the cases of coPVP and PVP indicating that the ASDs prepared by these two polymers are more prone to amorphous-amorphous demixing and API recrystallization in the presence of moisture.

3.3. Molecular interaction

One crucial factor for ASD physical stability, leading to greater recrystallization resistance, is thermoplastic polymer's ability to offer complementary hydrogen-bonding sites to the API. Hence, in order to full comprehend the underlying forces leading to ASD stabilization it is crucial to evaluate for hydrogen bonds (H-bonds) between the API and the polymeric carrier.

3.3.1. Molecular dynamics simulations

In a first step, the presence of molecular interactions between RXB and the selected polymers, was evaluated theoretically with the aid of MD simulations. Fig. 9 shows the representative molecular structures of all ASDs during the MD simulations process, where molecular interactions between the API and all thermoplastic polymers is predicted. Specifically, MD simulations suggested that H-bonds are being formed between the secondary amide groups of RXB and the C═O groups of the selected polymers.

3.3.2. DSC results

In order to experimentally verify the presence of molecular interactions suggested by MD simulations, DSC experiments were conducted (Figure S3, supplementary material). Results showed that the recorded Tg values decrease as the content of the API increases. This could be the result of strong interactions taking place among the reactive groups of the polymers and the API. Fig. 10 shows the comparison of Tg vs.

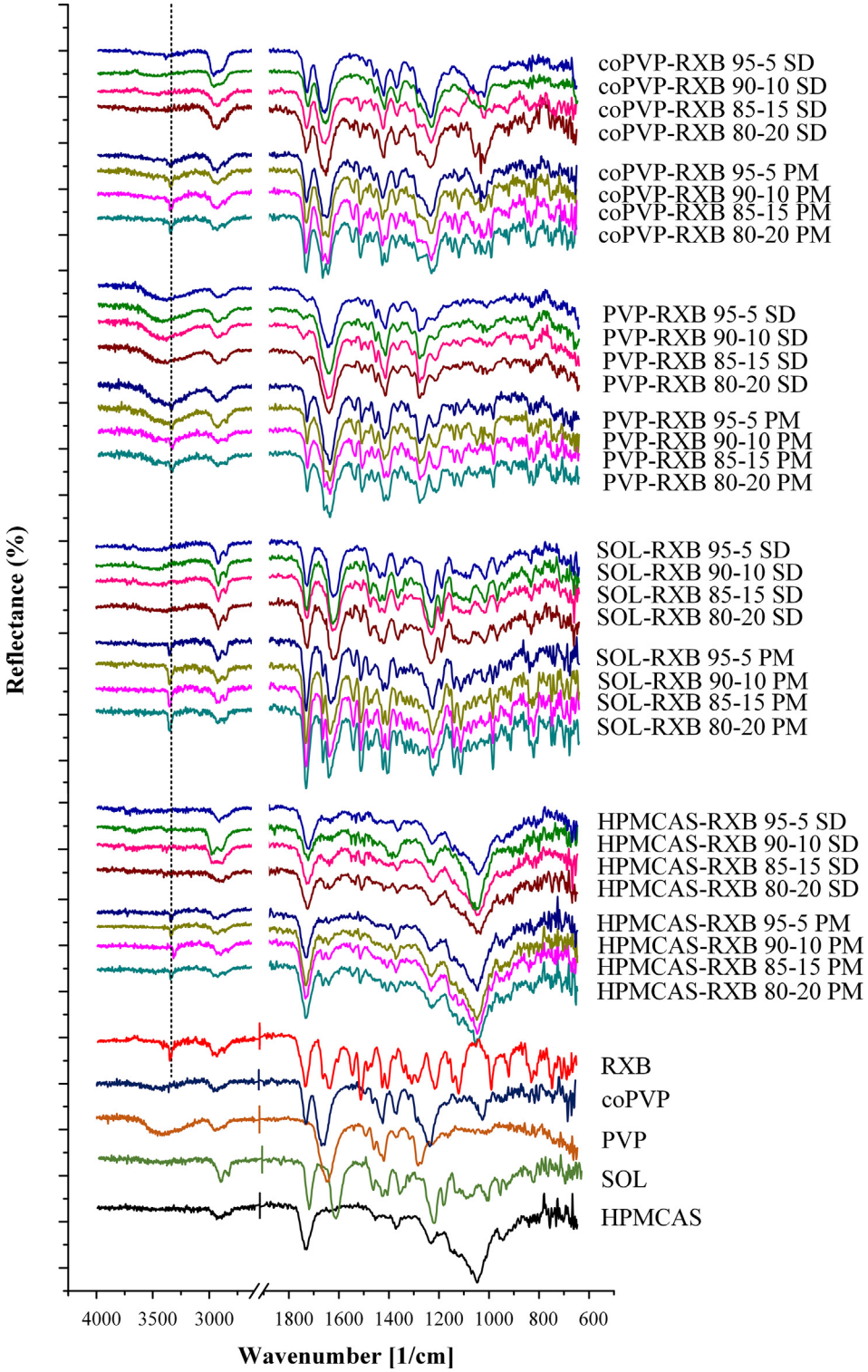

Fig. 11. ATR-FTIR spectra of RXB, coPVP, PVP, SOL, HPMCAS, RXB-polymer physical mixtures (PM) and solid dispersions (SD).

composition profile of all ASD systems for the experimentally determined Tg values and the Tg values estimated theoretically via Gordon-Taylor (GT) equation, where the significant deviation between the two Tg values verifies the formation of molecular interactions between the two components in all cases. Specifically, in contrary to PVP based ASDs, in the case of RXB ASD with coPVP, SOL and HPMCAS, a negative deviation of the experimentally determined Tg values was observed compared to the GT estimations, indicating that probably homonuclear interactions were stronger in these systems compared to heteronuclear interactions [46]

3.3.3. ATR-FTIR results

Finally, in order to further evaluate the molecular interactions occurring among ASD components, ATR-FTIR analysis was conducted. Fig. 11 shows the ATR-FTIR spectra of the pure components, the physical mixtures (PMs) and the prepared ASD. Specifically, regarding the pure components, coPVP showed characteristics peaks at: 1450–1480 cm^{-1} corresponding to C—C binding, and 1690 and

1750 cm^{-1} corresponding to ν(C═O) of the 1-vinyl-2-pyrrolidone and vinyl acetate, respectively; PVP displayed absorption bands at: 3450 cm^{-1} corresponding to absorbed water, 2960 cm^{-1} corresponding to ν(C-H), 1672 and 1657 cm^{-1} corresponding to ν(C═O), 1441 and 1379 cm^{-1} corresponding to (δCH_2) and 1294 cm^{-1} corresponding to ν(C-N); SOL showed characteristics peaks at: 2913 cm^{-1}, 1725 cm^{-1} and 1628 cm^{-1}, corresponding to the −CH and −C═O stretching of –OC(O)CH_3 or ester group (1725 cm^{-1}) and the stretching of −C(O)N or amide group (1625 cm^{-1}), respectively; HPMCAS showed characteristics peaks at: 1694 cm^{-1} corresponding to the C−O vibrations of the carboxylic groups and at 2500–3500 cm^{-1} corresponding to the hydroxyl groups of the polymer; while RXB showed characteristic peaks at 3355 cm^{-1} corresponding to secondary amide (N-H) stretching vibration, 1740 cm^{-1} corresponding to C═O stretching from the ester group, 1670–1640 cm^{-1} corresponding to the amide group stretching, 1300–1000 cm^{-1} corresponding to the C−O−C movement present in both ethers and esters and 850–550 cm^{-1} corresponding to C−Cl stretching.

Comparison of FTIR spectra between the PMs and the corresponding SDs showed that in all cases the secondary amide (N−H) peak of the API (located at 3355 cm^{-1}, dashed line in Fig. 11) disappears, indicating the presence of molecular interactions between the API and the tested polymers. Specifically, in the case of RXB-coPVP ASDs, in addition to the missing −NH stretching peak, FTIR spectra showed a shift in polymer's C═O peak from 1690 to 1675 cm^{-1}, indicating that the −NH groups of the API are probably forming H-bonds with the C═O groups of the 1-vinyl-2-pyrrolidone part of coPVP. Analogous shifts for the FTIR peaks of RXB-PVP ASDs were also recorded indicating the formation of similar H-bonds between the two components. In the case of RXB-SOL ASDs, several spectra changes were recorded in the region of 1750–1600 cm^{-1}, indicating that the API's secondary amide groups are probably forming H-bonds with the −C═O groups of SOL, while, in the case of RXB-HPMCAS ASDs, in addition to the missing RXB −NH stretching peak, the shift (at lower wavenumbers) of the peak corresponding to HPMCAS's carboxylic groups, indicates the formation of H-bonds between the two components.

Therefore, based on the above, FTIR spectra analysis verifies the formation of H-bonds between the API and the selected thermoplastic polymers suggested by MD simulations.

4. Conclusion

Since RH has a tremendous impact on the physical stability of ASD systems, and especially in the molecular state of the API within the polymeric matrix (i.e. whether it is amorphously dispersed within the polymer, or it is demixed into two amorphous phases (API-amorphous and polymer-amorphous), or it is recrystallized within the matrix), in the present study, moisture-induced thermodynamic phase diagrams were constructed for several RXB ASD systems with the aid of FH lattice theory. Verification experiments were in agreement with the theoretically constructed phase diagrams (under zero and elevated RH conditions), showing that SOL and HPMCAS ASDs were more stable compared to coPVP and PVP. Keeping in mind that in all prepared systems strong molecular interactions between the API and the selected polymers were verified both theoretically (via MD simulations) and experimentally (via DSC and FTIR), it is the presence of moisture water and its effect on the physicochemical properties of the ASD that leads to these physical stability differences.

Declaration of interest

The authors report no declarations of interest.

Appendix A. Supplementary data

Supplementary data to this article can be found online at https://doi.org/10.1016/j.ejpb.2019.10.010.

References

[1] K. AboulFotouh, A.A. Allam, M. El-Badry, A.M. El-Sayed, Role of self-emulsifying drug delivery systems in optimizing the oral delivery of hydrophilic macromolecules and reducing interindividual variability, Colloids Surf. B., Biointerf. 167 (2018) 82–92.
[2] A. Bhakay, M. Rahman, R.N. Dave, E. Bilgili, Bioavailability enhancement of poorly water-soluble drugs via nanocomposites: formulation(-)processing aspects and challenges, Pharmaceutics 10 (2018).
[3] C. Brough, R.O. Williams, Amorphous solid dispersions and nano-crystal technologies for poorly water-soluble drug delivery, Int. J. Pharmaceut. 453 (2013) 157–166.
[4] R.L. Carrier, L.A. Miller, I. Ahmed, The utility of cyclodextrins for enhancing oral bioavailability, J. Control. Release 123 (2007) 78–99.
[5] L. Di, P.V. Fish, T. Mano, Bridging solubility between drug discovery and development, Drug Discovery Today 17 (2012) 486–495.
[6] M. Li, M. Azad, R. Dave, E. Bilgili, Nanomilling of drugs for bioavailability enhancement: a holistic formulation-process perspective, Pharmaceutics 8 (2016).
[7] M. Reddy, S. Sowmya, S.M.F.U. Haq, Formulation and in-vitro characterization of self microemulsifying drug delivery systems of rivaroxaban, Int. J. Pharmaceut. Sci. Res. 8 (2017) 3436–3445.
[8] I. Sathisaran, S.V. Dalvi, Engineering cocrystals of poorlywater-soluble drugs to enhance dissolution in aqueous medium, Pharmaceutics 10 (2018).
[9] A. Haser, F. Zhang, New strategies for improving the development and performance of amorphous solid dispersions, AAPS PharmSciTech 19 (2018) 978–990.
[10] D. Lin, Y. Huang, A thermal analysis method to predict the complete phase diagram of drug–polymer solid dispersions, Int. J. Pharm. 399 (2010) 109–115.
[11] T. Van Duong, G. Van den Mooter, The role of the carrier in the formulation of pharmaceutical solid dispersions. Part II: amorphous carriers, Exp. Opin. Drug Deliv. 13 (2016) 1681–1694.
[12] K. Edueng, D. Mahlin, C.A.S. Bergström, The need for restructuring the disordered science of amorphous drug formulations, Pharm. Res. 34 (2017) 1754–1772.
[13] X. Lin, Y. Hu, L. Liu, L. Su, N. Li, J. Yu, B. Tang, Z. Yang, Physical stability of amorphous solid dispersions: a physicochemical perspective with thermodynamic, kinetic and environmental aspects, Pharmaceut. Res. 35 (2018) 125.
[14] P. Piccinni, Y. Tian, A. McNaughton, J. Fraser, S. Brown, D.S. Jones, S. Li, G.P. Andrews, Solubility parameter-based screening methods for early-stage formulation development of itraconazole amorphous solid dispersions, J. Pharm. Pharmacol. 68 (2016) 705–720.
[15] N. Fan, P. Ma, X. Wang, C. Li, X. Zhang, K. Zhang, J. Li, Z. He, Storage stability and solubilization ability of HPMC in curcumin amorphous solid dispersions formulated by Eudragit E100, Carbohydr. Polym. 199 (2018) 492–498.
[16] S. Wang, C. Liu, Y. Chen, A.D. Zhu, F. Qian, Aggregation of hydroxypropyl methylcellulose acetate succinate under its dissolving pH and the impact on drug supersaturation, Mol. Pharm. (2018).
[17] D. Medarevic, S. Cvijic, V. Dobricic, M. Mitric, J. Djuris, S. Ibric, Assessing the potential of solid dispersions to improve dissolution rate and bioavailability of valsartan: in vitro-in silico approach, Eur. J. Pharmaceut. Sci. Off. J. Eur. Fed. Pharmaceut. Sci. (2018).
[18] E.S. Bochmann, K.E. Steffens, A. Gryczke, K.G. Wagner, Numerical simulation of hot-melt extrusion processes for amorphous solid dispersions using model-based melt viscosity, Eur. J. Pharmaceut. Biopharmaceut.: Off. J. Arbeitsgemeinschaft fur Pharmazeutische Verfahrenstechnik e.V 124 (2018) 34–42.
[19] J.S. Chae, B.R. Chae, D.J. Shin, Y.T. Goo, E.S. Lee, H.Y. Yoon, C.H. Kim, Y.W. Choi, Tablet formulation of a polymeric solid dispersion containing amorphous alkalinized Telmisartan, AAPS PharmSciTech (2018).
[20] T.M. Deshpande, A. Quadir, S. Obara, S.W. Hoag, Impact of formulation excipients on the thermal, mechanical, and electrokinetic properties of hydroxypropyl methylcellulose acetate succinate HPMCAS, Int J Pharm 542 (2018) 132–141.
[21] K. Lehmkemper, S.O. Kyeremateng, M. Bartels, M. Degenhardt, G. Sadowski, Physical stability of API/polymer-blend amorphous solid dispersions, Eur. J. Pharm. Biopharm. 124 (2018) 147–157.
[22] K. Lehmkemper, S.O. Kyeremateng, O. Heinzerling, M. Degenhardt, G. Sadowski, Impact of polymer type and relative humidity on the long-term physical stability of amorphous solid dispersions, Mol. Pharm. 14 (2017) 4374–4386.
[23] S. Dalsania, J. Sharma, B. Munjal, A.K. Bansal, Impact of drug-polymer miscibility on enthalpy relaxation of Irbesartan amorphous solid dispersions, Pharm. Res. 35 (2018) 29.
[24] D.E. Moseson, L.S. Taylor, The application of temperature-composition phase diagrams for hot melt extrusion processing of amorphous solid dispersions to prevent residual crystallinity, Int. J. Pharm. 553 (2018) 454–466.
[25] M. Remko, Molecular structure, lipophilicity, solubility, absorption, and polar surface area of novel anticoagulant agents, J. Mol. Struct. (Thoechem) 916 (2009) 76–85.
[26] M. Ganesh, Design and optimization of rivaroxaban lipid solid dispersion for dissolution enhancement using statistical experimental design, Asian J. Pharmaceut. 10 (2016) 59–64.
[27] S. Metre, S. Mukesh, S.K. Samal, M. Chand, A.T. Sangamwar, Enhanced biopharmaceutical performance of rivaroxaban through polymeric amorphous solid dispersion, Mol. Pharm. 15 (2018) 652–668.
[28] P.J. Marsac, S.L. Shamblin, L.S. Taylor, Theoretical and practical approaches for prediction of drug-polymer miscibility and solubility, Pharm. Res. 23 (2006) 2417–2426.

[29] T.C. Frank, J.R. Downey, S.K. Gupta, Quickly screen solvents for organic solids, Chem. Eng. Prog. 95 (1999) 41–61.
[30] O. Trott, A.J. Olson, AutoDock Vina: improving the speed and accuracy of docking with a new scoring function, efficient optimization and multithreading, J. Comput. Chem. 31 (2010) 455–461.
[31] G.M. Morris, D.S. Goodsell, R.S. Halliday, R. Huey, W.E. Hart, R.K. Belew, A.J. Olson, Automated docking using a Lamarckian genetic algorithm and an empirical binding free energy function, J. Comput. Chem. 19 (1998) 1639–1662.
[32] Y. Tian, J. Booth, E. Meehan, D.S. Jones, S. Li, G.P. Andrews, Construction of drug-polymer thermodynamic phase diagrams using Flory-Huggins interaction theory: identifying the relevance of temperature and drug weight fraction to phase separation within solid dispersions, Mol. Pharm. 10 (2013) 236–248.
[33] M. Gordon, J.S. Taylor, Ideal copolymers and the second-order transitions of synthetic rubbers. I. non-crystalline copolymers, J. Appl. Chem. 2 (1952) 493–500.
[34] C. Luebbert, M. Wessner, G. Sadowski, Mutual impact of phase separation/crystallization and water sorption in amorphous solid dispersions, Mol. Pharm. 15 (2018) 669–678.
[35] A. Prudic, Y. Ji, C. Luebbert, G. Sadowski, Influence of humidity on the phase behavior of API/polymer formulations, Eur. J. Pharm. Biopharm. 94 (2015) 352–362.
[36] K. Lehmkemper, S.O. Kyerematen, O. Heinzerling, M. Degenhardt, G. Sadowski, Long-term physical stability of PVP- and PVPVA-amorphous solid dispersions, Mol. Pharm. 14 (2017) 157–171.
[37] J. Sun, X. Liu, Z. Fang, S. Mao, L. Zhang, S. Rohani, J. Lu, Solubility measurement and simulation of rivaroxaban (Form I) in solvent mixtures from 273.15 to 323.15 K, J. Chem. Eng. Data 61 (2016) 495–503.
[38] B.C. Hancock, G. Zografi, The use of solution theories for predicting water vapor absorption by amorphous pharmaceutical solids: a test of the Flory-Huggins and Vrentas models, Pharm. Res. 10 (1993) 1262–1267.
[39] K. Punčochová, J.Y.Y. Heng, J. Beránek, F. Štěpánek, Investigation of drug–polymer interaction in solid dispersions by vapour sorption methods, Int. J. Pharm. 469 (2014) 159–167.
[40] D.R. Sturm, S.-W. Chiu, J.D. Moser, R.P. Danner, Solubility of water and acetone in hypromellose acetate succinate, HPMCAS-L, Fluid Phase Equilibria 429 (2016) 227–232.
[41] P. Barmpalexis, A. Karagianni, K. Kachrimanis, Molecular simulations for amorphous drug formulation: Polymeric matrix properties relevant to hot-melt extrusion, Eur. J. Pharm. Sci.: Off. J. Eur. Fed. Pharm. Sci. 119 (2018) 259–267.
[42] W.F.V. Gunsteren, A.E. Mark, Validation of molecular dynamics simulations, J. Chem. Phys. 108 (1998) 6109–6116.
[43] P. Barmpalexis, A. Karagianni, I. Nikolakakis, K. Kachrimanis, Preparation of pharmaceutical cocrystal formulations via melt mixing technique: a thermodynamic perspective, Eur. J. Pharm. Biopharm. 131 (2018) 130–140.
[44] A. Newman, E. Munson, Characterizing miscibility in amorphous solid dispersions, Am. Pharm. Rev. 15 (2012) 92–108.
[45] X. Yuan, D. Sperger, E.J. Munson, Investigating miscibility and molecular mobility of nifedipine-PVP amorphous solid dispersions using solid-state NMR spectroscopy, Mol. Pharm. 11 (2014) 329–337.
[46] S. Baghel, H. Cathcart, N.J. O'Reilly, Polymeric amorphous solid dispersions: a review of amorphization, crystallization, stabilization, solid-state characterization, and aqueous solubilization of biopharmaceutical classification system class II drugs, J. Pharm. Sci. 105 (2016) 2527–2544.